Journal of Volcanology and Geothermal Research 454 (2024) 108173

Contents lists available at ScienceDirect

Journal of Volcanology and Geothermal Research

journal homepage: www.journals.elsevier.com/journal-of-volcanology-and-geothermal-research

Source analysis of low frequency seismicity at Mt. Vesuvius by a hybrid moment tensor inversion

R. Manzo [a,b,*], S. Cesca [c], D. Galluzzo [a], M. La Rocca [d], M. Picozzi [e], R. Di Maio [b]

[a] National Institute of Geophysics and Volcanology, Naples Section, Vesuvius Observatory, Naples, Italy
[b] Department of Earth, Environment and Resources Sciences, University of Naples Federico II, Naples, Italy
[c] GFZ German Research Centre for Geosciences, Potsdam, Germany
[d] University of Calabria, Rende, (CS), Italy
[e] Department of Physics E. Pancini, University of Naples Federico II, Naples, Italy

ARTICLE INFO

Keywords:
Volcano seismology
Earthquake source
Low frequency signals
Moment tensor
Mt. Vesuvius

ABSTRACT

Seismicity at Mt. Vesuvius has been relatively weak in the last decades. While the occurrence of shallow volcano-tectonic (VT) events at Mt. Vesuvius is well known, the occurrence of deeper low frequency events (LF) was only recently recognized. Previous source studies only targeted VT events, which were found to have quite heterogeneous focal mechanisms. In this paper, we perform for the first time the source inversion of LF seismicity at Mt. Vesuvius, analysing 27 LF events recorded from 2012 to 2021 with the aim to investigate their source processes. Given the challenges of analysing weak LF earthquakes, we implement a specific moment tensor (MT) inversion approach that combines the fit of displacement seismograms in the time domain and amplitude spectra in the frequency domain. The inversion is simultaneously performed for the source depth and moment tensor components in the 2–7 and 2–5 Hz frequency band, assuming either a full or deviatoric MT representation. Source parameter uncertainties are estimated by using a Bayesian bootstrapping scheme. Our results confirm a larger depth of LF events compared to VTs and show a strong heterogeneity of the LF seismic sources, which present various rupture types, different orientations and heterogeneous, whilst poorly resolved, non-double-couple components. The MT variability is qualitatively confirmed by significant differences among the recorded waveforms. The heterogeneity of both VT and LF source processes is attributed to complex source processes in a highly fractured seismogenic volume submitted to a heterogeneous stress field.

1. Introduction

Understanding seismogenic processes and their source in volcanic environments is one of the main goals of volcano seismology. The identification, location and characterization of the sources of different types of seismic signals recorded at volcanoes is helpful for understanding the volcanic plumbing system and its dynamics (Neuberg, 2000). The link between earthquakes and volcanic eruptions dates back to the time of Plinio il Giovane, who first gave a description of a volcanic eruption: the 79 CE eruption at Mt. Vesuvius (Naples, Southern Italy). Historically, Mt. Vesuvius has played a central role in the study of seismic signals associated with volcanic activity. Indeed, it was the first volcano whose earthquakes were mentioned in the scientific literature, the first to have an observatory since 1847, and the first to be monitored with specific seismological equipment (i.e., the Palmieri electromagnetic seismograph, built in 1862, which was the first seismic instrument to record volcanic seismicity). A first quantitative description of seismicity associated with volcanic activity for the 1944 eruption of Mt. Vesuvius was provided by Imbò (1952).

Research focused on the relationship between volcanic earthquakes and eruptive processes provided a classification of different types of seismic events (Chouet, 1996; Zobin, 2012). Zobin (2012), in particular, classified volcanic earthquakes into two general groups. The first, defined as volcano-tectonic (VT), comprises all those earthquakes controlled by stress field perturbations during the migration of magma in the Earth's crust. The second group includes all those earthquakes caused by magmatic activity within volcanic conduits and reservoirs; these are called eruption earthquakes. According to Chouet (1996), the most common types of seismic events occurring in volcanic areas are: 1) high frequency (HF) events or VTs; 2) earthquakes associated with

* Corresponding author at: National Institute of Geophysics and Volcanology Naples Section, Vesuvius Observatory, Naples, Italy.
E-mail addresses: roberto.manzo@unina.it, roberto.manzo@ingv.it (R. Manzo).

https://doi.org/10.1016/j.jvolgeores.2024.108173
Received 18 January 2024; Received in revised form 30 July 2024; Accepted 18 August 2024
Available online 20 August 2024

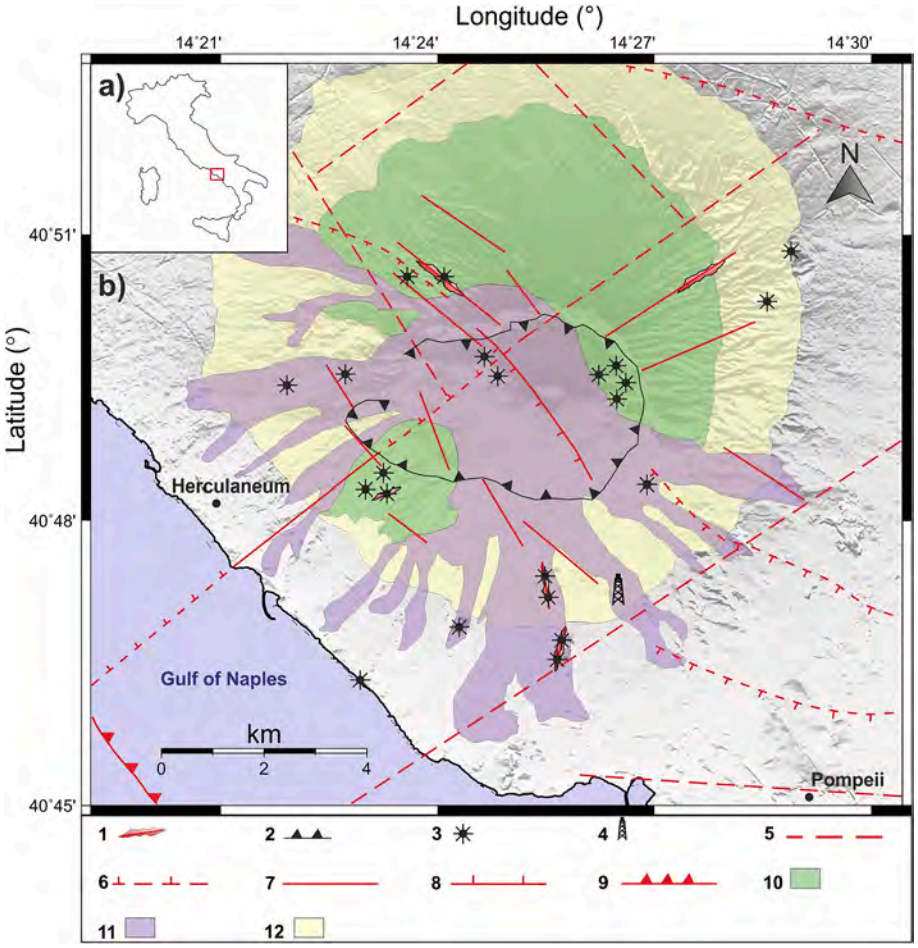

Fig. 1. a) Mt. Vesuvius area in Southern Italy. b) Structural and volcanological sketch map of the Somma-Vesuvius volcanic complex (modified from Bianco et al., 1998 and D'Auria et al., 2014). 1) Eruptive fractures; 2) Somma caldera rim; 3) Eruptive vents; 4) Trecase well; 5) Carbonatic basement faults; 6) Quaternary faults; 7) Recent faults of the Somma-Vesuvius complex; 8) Vesuvius crater fault; 9) Thrusting evidence; 10) Somma lavas and minor pyroclastics and Vesuvius pyroclastics; 11) Vesuvius lavas; 12) Quaternary sediments.

explosive activity (explosion quakes); 3) volcanic tremor; and 4) low frequency (LF) or long period (LP) events, with different subcategories [i.e., very-long or ultra-long period (VLP or ULP) events], depending on the predominant frequency. VT earthquakes are generally interpreted as the result of fracturing and shear faulting. The latter show seismic signals with clear P and S onsets, similar to tectonic earthquakes. Typical VTs seismograms have dominant frequencies between 5 and 20 Hz (Wassermann, 2009). VT focal mechanisms may exhibit anomalous source characteristics, such as non-double-couple source components (e.g. Saraò et al., 2001; Templeton and Dreger, 2006; Büyükakpinar et al., 2023; Del Fresno et al., 2023), which may imply greater complexity in the earthquake genesis process. Explosion quakes and their signals are highly dependent on the type and style of explosive activity, i.e., strombolian or volcanic explosions and phreatomagmatic explosions, where signals are characterized by both high and low frequency pulses (Zobin, 2012). In recent years, these earthquakes have also been studied using infrasonic microphones or pressure sensors to complement seismic networks and provide a more complete picture of some explosive and eruptive processes (Zobin, 2012). The increasing use of sensitive seismic instruments installed on active volcanoes has allowed the recording of another type of seismic signal, referred to as "volcanic tremor". The latter is characterized by continuous vibrations that can last for minutes, days or even months and are closely related to the volcanic activity (Wassermann, 2009). Volcanic tremor has been observed at many volcanoes both before and during eruptions (McNutt, 2005) and has been linked to fluid movement within the feeding system. The last category of seismic signals in volcanic areas is represented by low-frequency (LF) events. LF records have lower dominant frequencies (1–5 Hz) compared to VTs, and they often lack impulsive body wave onset. LFs have been widely observed in the context of magmatic and hydrothermal activity in volcanic areas (Saccorotti et al., 2007) and are often interpreted as being generated by the resonance of conduits and reservoirs in response to fluid transfer, inflation or depletion processes. In some cases, they have been recognized as precursors of eruptive activity (Chouet, 1996, 2003). The waveforms of some LF events are typically characterized by damped harmonic oscillations (e.g., 'tornillos'). Unlike VT events, LF seismicity is often difficult to localize using conventional methods due to the lack of impulsive phases (Wassermann, 2009).

After the last eruption occurred in 1944, the seismicity at Mt. Vesuvius has been quite low and characterized by low magnitude VT earthquakes (Bianco et al., 1998; D'Auria et al., 2014; Cusano et al., 2022), while low-frequency earthquakes have only recently been identified (La Rocca and Galluzzo, 2016; Galluzzo et al., 2020; Galluzzo et al., 2022). Seismicity studies at Mt. Vesuvius remain challenging due to the low magnitude of the earthquakes, high background noise, and complexity of the seismic signals. The methodologies used in the past to analyse the source mechanisms of Mt. Vesuvius seismicity are mainly based on the polarity of the direct phases (P and S phases) (Bianco et al., 1998; D'Auria et al., 2014; Cusano et al., 2022). These approaches sometimes preclude the analysis of low magnitude earthquakes with emergent onset and low signal-to-noise ratio, typical features of the low-frequency signals recorded at Vesuvius. In this paper, we analyse the low

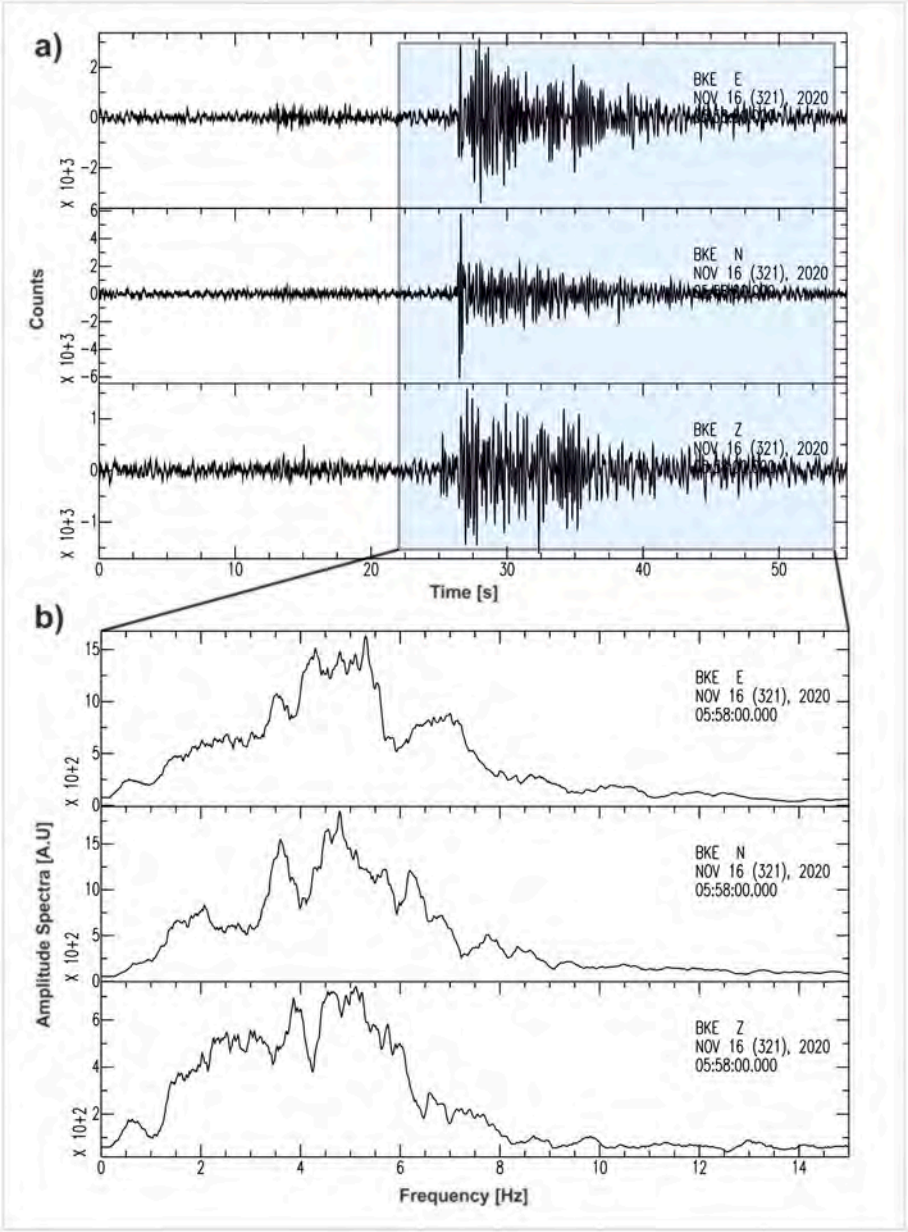

Fig. 2. a) Typical LF waveform in the time domain. The light blue box indicates the window in which the FFT (Fast Fourier Transform) is calculated. b) Amplitude Spectra of the LF event shown in a). (For interpretation of the references to colour in this figure legend, the reader is referred to the web version of this article.)

frequency seismicity to provide a broader view of the source processes at Mt. Vesuvius for the period 2012–2021. Our study focuses on recently identified low-frequency events that can be used to assess the short-term eruptive potential or the eruptive state of a volcano (Chouet et al., 1994). To overcome the modelling challenges described above, we propose a specific inversion approach that combines a robust probabilistic seismic source inversion scheme, careful data quality assessment and a specific data quality-driven waveform-based inversion setup.

2. Geological and volcanological background

Mt. Vesuvius in Southern Italy (Fig. 1a) is one of the most studied and best monitored volcanoes in the world. It is a stratovolcano located in the Campanian Plain depression between the eastern side of the Tyrrhenian Sea and the Southern Apennines chain (Brancaccio et al., 1991; Brocchini et al., 2001). The well-known Tyrrhenian 41st parallel line strike-slip faults system discontinuity (Spadini and Wezel, 1995; Lavecchia, 1988) separates the Somma-Vesuvius area from the Phlegraean Fields district (Ferrucci et al., 1989; Locardi and Nicolich, 1988). In the Late Pleistocene-Holocene, a significant subsidence of about 1 mm/yr occurred along the whole Tyrrhenian margin (Bianco et al., 1998), which was subsequently accompanied by an uplift phase of the Mesozoic carbonates bordering the Campanian Plain caused by faults with NW-SE/NNW-SSE and NNE-SSW/NE-SW trends (Fig. 1b) (Oldow et al., 1993; Hyppolite et al., 1994; Bianco et al., 1998; Ventura and Vilardo, 1999; Piochi et al., 2005). A complete stratigraphic record of the volcanic succession and sedimentary basement is available from the Trecase well (Fig. 1b), which is located in the SE Vesuvius sector and reaches a depth of 2072 m (Bernasconi et al., 1981; Zollo et al., 2002). From top to bottom, the succession is characterized by lava flows, pumices and tuffs down to the dolostones of the Mesozoic Apennine platform (Brocchini et al., 2001); leucite-bearing tephritic lavas at a depth of about 1221 m, dated at 0.369 ± 0.028 Myr ($^{40}Ar/^{39}Ar$), close the sequence and represent the oldest products of the Somma-Vesuvius

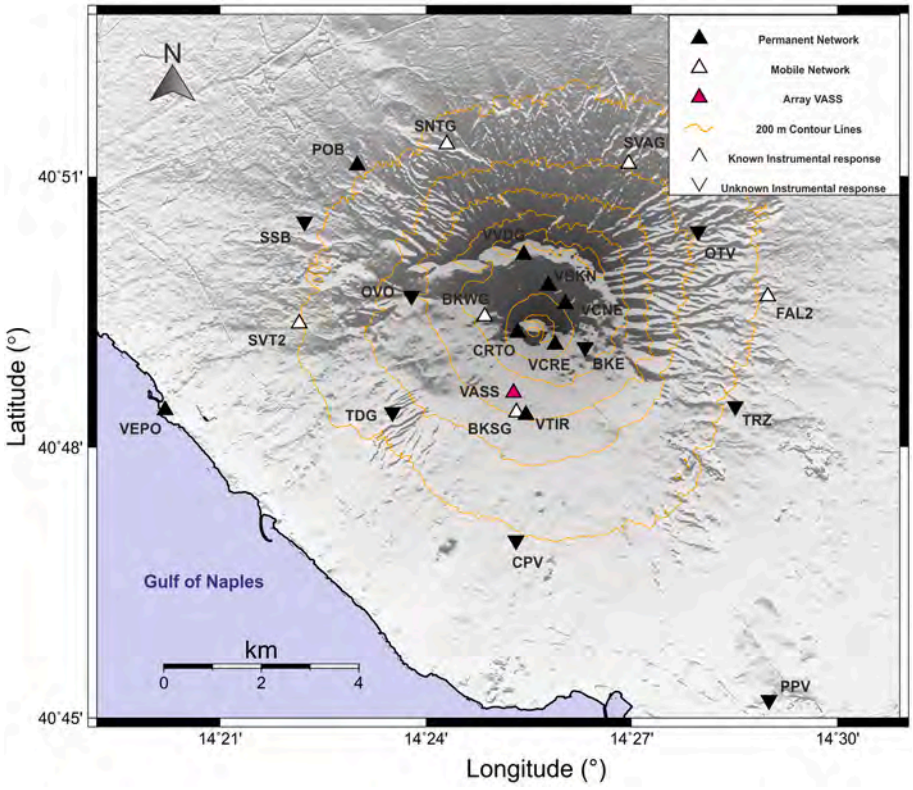

Fig. 3. The actual seismic monitoring network operating on Mt. Vesuvius. The magenta triangle marks the Vesuvius Array South Stacking (VASS) array. The sensor characteristics of the network are described in Orazi et al. (2013) and La Rocca and Galluzzo (2014, 2015). (For interpretation of the references to colour in this figure legend, the reader is referred to the web version of this article.)

Table 1
The 1D velocity model used to localize LF events.

*Depth (km)	V_P (km/s)	V_S (km/s)
0	3.0	1.6
1.2	4.5	2.4
7.2	6.0	3.3
Half space	6.5	3.7

* Depth is calculated from the top of Mt. Vesuvius.

eruptive activity that began about 300–500 ka ago (Santacroce, 1987). Nevertheless, the outcropping volcanic products show ages no older than 25 kyr. In fact, the eruptive history of Vesuvius during this period was very complex and troubled, characterized by plinian eruptive phases, subplinian eruptions, minor strombolian and effusive activity and quiescent periods. The eruptive history of this volcano has therefore certainly involved a continuous morphological transformation of the entire volcanic area. Initially, the volcanic edifice consisted of an old and continuously collapsing stratovolcano (Mt. Somma) and a young cone (Vesuvius). The main eruptive episodes studied by the worldwide scientific volcanological community are: Pomici di Base (18–20 kyr), Mercato (8.0 kyr), Avellino (3.9 kyr) and Pompei (79 CE) (Andronico et al., 1995). The latter is certainly the most famous and one of the best documented in the world, following the descriptions of 'Plinio il Giovane' in his two letters to the historian Tacitus. After the last Plinian eruption in 1631 (Rosi et al., 1993), Vesuvius was characterized by open-conduit activity, which ended with the last eruption occurring in 1944. Since then, it has entered a dormant phase, which is still ongoing.

3. Seismicity at Mt. Vesuvius

After the 1944 eruption, the Vesuvius seismicity was very low for about 20 years. Then, a significant increase in the number, energy and magnitude of earthquake was observed (Giudicepietro et al., 2010). Four distinct periods of high-rate seismicity occurred in 1978–1979, 1989–1990, 1995–1996 and 1999–2000, respectively. The strongest earthquake recorded at Vesuvius after 1944 (M_D 3.6) occurred on October 9, 1999 (D'Auria et al., 2013). Since the early 1999, the Vesuvius seismic network has recorded a variety of seismic events with about 21,000 transient signals whose sources are located in the volcanic area. Most of the seismicity at Mt. Vesuvius since 1999 occurs in two distinct seismogenic volumes at different depths. The first, shallower, is located above sea level and its seismicity is characterized by low magnitude ($M_D \leq 2.8$), the second, deeper seismogenic volume extends from 1.0 to 6.5 km depth.

Over the last two decades, most Volcano-Tectonic (VT) earthquakes have been of low magnitude ($M_D < 3$), sometimes occurring as low-energy swarms. Low-Frequency (LF) earthquakes have been identified by scanning continuous seismic signals, sometimes as single sporadic events and in other cases as short-lived volcanic tremor consisting of low-frequency swarms (La Rocca and Galluzzo, 2016). They were located at depths between 5 and 7 km below the volcanic cone. Petrosino and Cusano (2020) analyzed the seismicity of Mt. Vesuvius from 2003 to 2018 and recognized an atypical pattern, distinguishing several families of seismic events characterized by low-frequency spectral content (< 6 Hz). Other authors locate LFs between 5 and 7 km b.s.l., based on an almost constant time difference between P-wave (Tp) and S-wave (Ts) arrival times (Ts-Tp ~ 1.4 s) (La Rocca and Galluzzo, 2016; Galluzzo et al., 2020, 2022). Seismic signals of low magnitude VT earthquakes ($M_D \leq 2.8$) show spectral contents with peak frequency between 15 Hz and 22 Hz, while LF events have peak frequency between 2 and 6 Hz (La Rocca and Galluzzo, 2016).

Table 2
Deviatoric moment tensor inversion results for the 27 LF seismic events (ID) showing: origin time, centroid depth, moment magnitude (M_W), strike, dip and rake for the rupture plane, best and mean results for compensated linear vector dipole (CLVD), station number used for the inversion, azimuth gap, best frequency band and L1-norm misfit for the best solution. The best frequency band is the one that minimises the uncertainty for each event. The best CLVD values are obtained using all data with equal weight. Simultaneously, in order to estimate the uncertainties, the inversion is repeated for 100 data configurations with variable weights; these results are used to compute mean CLVD values and standard deviations. A significant difference between the mean and the best CLVD values indicates poorly resolved solutions.

ID	Origin Time (yyyymmdd hh:MM)	Latitude (°)	Longitude (°)	Depth (km)	M_W	Strike (°)	Dip (°)	Rake (°)	CLVD Best (%)	CLVD Mean (%)	Station number	Azimuth Gap (°)	Best frequency band (Hz)	L1-norm misfit
1	20120511 01:06	40.822	14.423	6.3	1.5	242	44	−36	−5	14 (−23; +51)	13	106	2–5	0.55
2	20130430 01:30	40.825	14.424	7.3	1.6	326	59	−60	−57	−8 (−49; +33)	10	137	2–7	0.50
3	20130430 02:00	40.821	14.427	7.8	1.5	236	67	−176	56	41 (+7; +75)	13	101	2–5	0.3
4	20130430 02:02	40.820	14.422	5.5	1.1	317	84	147	−57	−1 (−49; +47)	12	91	2–7	0.45
5	20130510 00:56	40.823	14.452	4.5	0.9	334	44	−106	9	26 (−10; +62)	8	123	2–7	0.4
6	20131218 16:26	40.813	14.440	7.7	1.7	51	48	−81	42	10 (−37; +57)	8	94	2–7	0.4
7	20140115 07:50	40.820	14.422	7.4	1.6	298	55	−86	47	7 (−38; +52)	7	106	2–7	0.38
8	20140228 07:56	40.802	14.433	4.8	1.1	84	61	67	−66	0 (−43; +43)	8	115	2–7	0.45
9	20140228 08:02	40.820	14.412	7.7	1.8	249	77	−180	−53	−36 (−75; +3)	6	118	2–7	0.45
10	20140829 03:32	40.820	14.411	7.8	1.4	273	87	−9	−78	−35 (−80; +10)	8	123	2–5	0.35
11	20141208 02:28	40.812	14.406	4.2	0.6	249	74	−44	89	9 (−36; +54)	12	190	2–7	0.6
12	20160221 19:10	40.827	14.404	7.8	1.7	236	62	−11	69	24 (−19; +67)	11	152	2–5	0.4
13	20180127 19:52	40.832	14.434	4.1	1.1	263	64	−16	62	28 (−13; +69)	6	232	2–7	0.45
14	20180127 21:14	40.823	14.412	4.7	1.0	262	63	164	57	18 (−21; +57)	7	107	2–5	0.4
15	20180127 21:18	40.826	14.420	6.2	1.0	127	72	124	−54	−9 (−53; +35)	7	67	2–5	0.4
16	20180330 00:16	40.829	14.425	7.6	1.2	282	52	149	−12	−4 (−48; +40)	10	128	2–5	0.4
17	20180403 00:02	40.839	14.419	7.0	1.1	281	46	−68	−48	−14 (−55; +27)	6	277	2–7	0.4
18	20180610 14:06	40.822	14.432	7.1	1.5	314	74	−169	37	29 (+1; +57)	8	107	2–5	0.35
19	20191125 00:00	40.833	14.439	6.8	1.0	54	64	−142	55	47 (+17; +77)	10	82	2–7	0.42
20	20191125 00:32	40.825	14.409	7.7	1.4	131	69	−10	−48	−18 (−55; +19)	8	228	2–7	0.42
21	20200502 02:12	40.828	14.423	7.5	1.3	348	59	−95	−10	21 (−17; +59)	14	65	2–7	0.4
22	20200907 19:30	40.820	14.417	4.5	1.1	129	77	−38	20	22 (−17; +61)	7	80	2–7	0.5
23	20201116 05:57	40.819	14.422	7.8	1.7	310	88	177	10	−6 (−40; +28)	6	93	2–7	0.45
24	20201116 05:58	40.820	14.452	7.8	1.8	305	70	−14	−22	−12 (−53; +29)	7	128	2–5	0.4
25	20201116 05:59	40.822	14.456	7.0	1.7	260	69	−25	−49	−37 (−62; −12)	7	158	2–5	0.35
26	20201204 23:04	40.813	14.421	4.8	1.2	117	72	−31	54	25 (+20; +70)	10	91	2–7	0.5
27	20210402 15:28	40.825	14.409	7.8	1.5	247	75	5	−56	−23 (−71; +25)	9	128	2–5	0.5

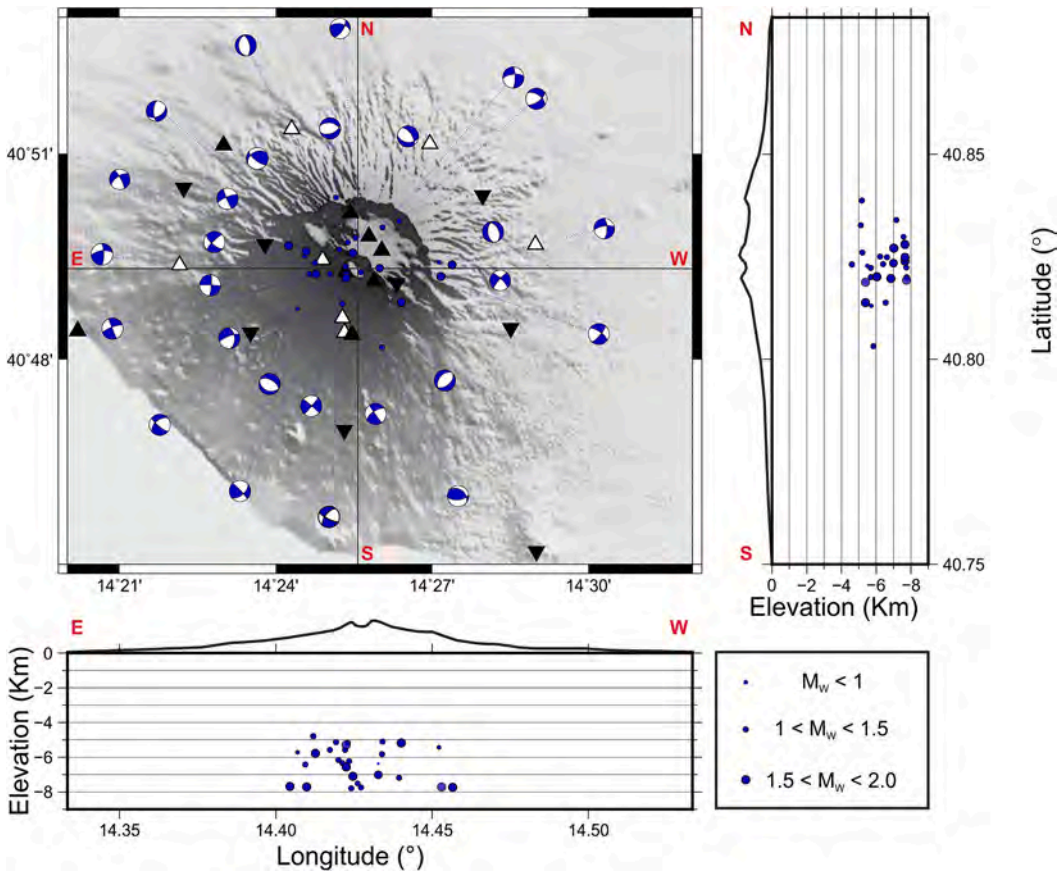

Fig. 4. Results of the deviatoric moment tensor (DMT) inversion. The blue circles represent the hypocenters of LF seismic events, whose size is proportional to the moment magnitude (M_W). (For interpretation of the references to colour in this figure legend, the reader is referred to the web version of this article.)

4. Data and methods

The dataset analyzed in this work by the moment tensor (MT) inversion consists of 27 low-frequency (LF) events recorded at Mt. Vesuvius from 2012 to 2021. These are single LF events, sometimes occurring within small swarm episodes, characterized by a frequency content between 2 and 7 Hz, centroid depths between 4.5 km and 7.5 km b.s.l. and magnitude (M_D) ranging from 0.6 to 1.8. A typical LF waveform at Mt. Vesuvius with its relative amplitude spectrum is shown in Fig. 2. The inversion procedure was applied to those earthquakes recorded by at least 6 stations with good azimuthal coverage and whose P- and S-phases could be identified with reasonably small uncertainty, given the background noise and the emergent onset. Most of the LF events analyzed in this work have been previously identified and used for other types of analyses (La Rocca and Galluzzo, 2016; Galluzzo et al., 2020, 2022).

At present, the seismic monitoring network at Mt. Vesuvius consists of single- and three-component short-period sensors, broadband digital sensors, accelerometers and infrasonic microphones (Orazi et al., 2013). The current development of the network and its geometry (Fig. 3) allow the localization of seismic events with $M_D < 1$ under conditions of low seismic noise. The magenta triangle in Fig. 3 represents the Vesuvius Array South Stacking (VASS) array that operated from 2012 to 2017 (La Rocca and Galluzzo, 2014). After signal stacking, VASS data are generally less noisy signals than other acquisition sites. Due to the use of old analogue in the last decades, for some recordings the parameters to convert the amplitude from counts to ground velocity are not known with sufficient precision.

In recent years, the seismic monitoring of Mt. Vesuvius has been enhanced by increasing the number of seismic stations and instrument performances, with great benefits for the data quality. Meanwhile, advanced data analysis techniques have been developed to investigate the origin and features of the recorded seismic signals and their relationship with the volcano dynamics. Among the widely used tools for seismic source analysis, the MT inversion represents a key resource for understanding seismic processes in tectonic and volcanic earthquakes. However, the application of MT inversion techniques to the seismicity recorded at Mt. Vesuvius is challenging for several reasons: the low magnitude and low signal-to-noise ratio, the use of a simplified velocity model, and the lack of clear body waves in the case of LF events.

Generally, it is important to note that the diagonal elements of a moment tensor (*MT*) can signify a change in volume if the tensor's trace is non-zero (Stein and Wysession, 2003). Positive and negative trace values indicate increase and decrease in volume, respectively. When the tensor's trace is non-zero, the moment tensor can be decomposed as follows:

$$MT = MT_{\mathrm{dev}} + MT_{\mathrm{iso}} \quad (1)$$

This decomposition is unique. MT_{iso} is a diagonal tensor with identical elements; MT_{dev} has a zero trace and five independent components. The latter can be further decomposed, although this decomposition is not unique (Jost and Herrmann, 1989). The most commonly used decomposition is:

$$MT_{\mathrm{dev}} = \mathrm{DC} + \mathrm{CLVD} \quad (2)$$

where DC represents a double-couple focal mechanism, describing pure shear failure, and the CLVD is the compensated linear vector dipole component, representing a deforming source without volume change (Frohlich, 1992; Julian et al., 1998). Non-double-couple sources are frequently observed, for instance, in volcanoes or specific processes such as landslides or mining collapses. Source mechanisms of tectonic

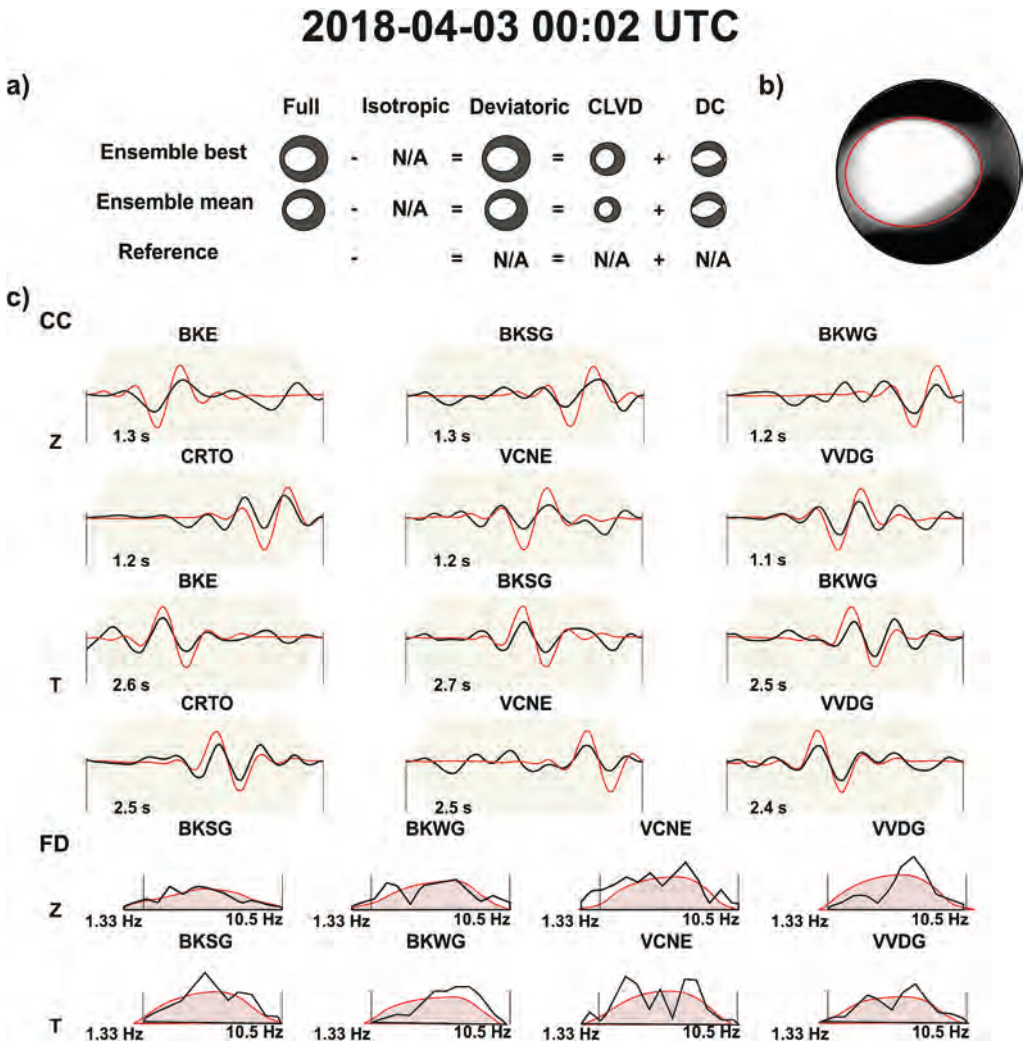

Fig. 5. Deviatoric moment tensor inversion results for the LF seismic event of 2018-04-03 (ID 17) in the frequency band 2–7 Hz. a) Decomposition of the best and mean MT solution into DC and CLVD components. (b) Beach ball illustrating the uncertainty of the best MT solution. (c) Examples of Cross-Correlation (CC) Fits and Frequency domain (FD) spectral fits at several stations. Synthetic and observed waveforms are represented by red and black lines, respectively. The beige-shaded area corresponds to the taper function. Station names are annotated above each panel. Numbers within the panels indicate waveform duration and frequency band for the amplitude spectra. (For interpretation of the references to colour in this figure legend, the reader is referred to the web version of this article.)

earthquakes are often interpreted using a double-couple model, which describes shear faulting. Conventionally, a full moment tensor (FMT) is often chosen for volcanological applications because it can describe isotropic, tensile, and shear sources, or a combination of these. The FMT is generally decomposed into an isotropic (ISO) and a deviatoric term (Knopoff and Randall, 1970). The ISO component represents the isotropic volume change in the focal region (Frohlich, 1992; Julian et al., 1998; Miller et al., 1998). The non-DC component (i.e., the sum of the isotropic and CLVD terms) is often small for tectonic earthquakes, which generally occur as shear failures. In volcanic environments, however, non-DC components can be generated by several physical processes, as for instance in response to fluid migration within the volcanic plumbing system and during overpressure conditions (Saraò et al., 2010).

4.1. Moment tensor inversion

In the present work, a hybrid moment tensor (MT) inversion approach, never used before for this seismicity, has been applied to LF signals. Obtaining MT solutions for magnitudes less than M_D 1.0 is not trivial; in this case it was possible thanks to the adoption of a specific inversion approach that combines the fit of seismograms in the time domain (fitting the data either with L1 norm or by cross-correlation) and in the frequency domain (fitting the amplitude spectra with L1 norm). The spectral fitting procedure was limited to those stations for which the transfer function was known. In this way, the use of the available waveform dataset can be maximized to achieve high robustness of the MT estimation. The open-software GROND (Heimann et al., 2018; Kühn et al., 2020), which implements Bayesian bootstrapping to estimate source parameter uncertainties, was used for the MT inversion. Seismic data were visually inspected to select only waveforms characterized by high signal-to-noise ratio, and only events well recorded by a sufficient number of seismic stations that provided a good azimuthal coverage. Synthetic seismograms (Heimann et al., 2019) were calculated using Green's functions computed with the QSEIS orthonormal propagation algorithm (Wang, 1999) adopting a 1D velocity model (Table 1) derived from the velocity model used for routine earthquake location (Lomax et al., 2001). We fitted 2 s time windows based on manual P and S wave picking. Synthetic seismogram time windows are automatically extracted based on theoretical arrival times. P-phases are fitted for the vertical component seismograms and S-phases for the two horizontal components. The inversion was performed both in the 2–5 Hz and 2–7 Hz frequency bands. For each earthquake, we choose the best frequency band as the one that minimises the average uncertainty of moment tensor components, as reported in Table 2. LF events are inverted for the

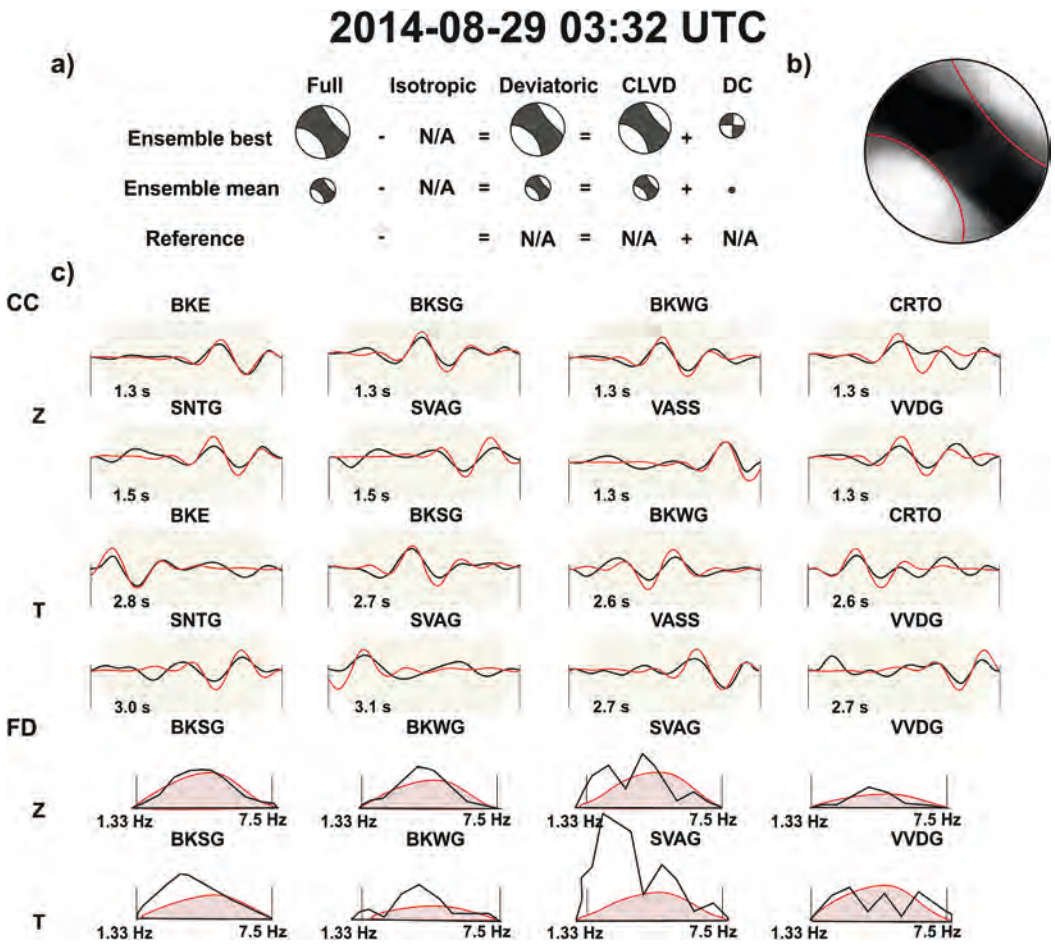

Fig. 6. Deviatoric moment tensor inversion results for the LF seismic event of 2014-08-29 (ID 10) in the frequency band 2–5 Hz. a) Decomposition of the best and mean MT solution into DC and CLVD components. (b) Beach ball illustrating the uncertainty of the best MT solution. (c) Examples of Cross-Correlation (CC) Fits and Frequency domain (FD) spectral fits at several stations. The beige-shaded area corresponds to the taper function. Station names are annotated above each panel. Numbers within the panels indicate waveform duration and frequency band for the amplitude spectra.

source depth and moment tensor components, assuming either a full or deviatoric MT representation. On this basis, we also estimate a moment magnitude and the MT decomposition, constraining the magnitude and depth search between −1 and 3.5 and between 4 km and 8 km, respectively which are considered realistic ranges for LFs at Mt. Vesuvius based on previous scientific literature mentioned in the Introduction section (Galluzzo et al., 2020, 2022). The optimization is setup to perform 100,000 iterations to ensure a stable convergence for all inverted source parameters. Finally, each input data was assigned the same weight (0.5), except for the VASS array, which was given a higher weight (1.0) because the stacking procedure improves the signal-to-noise ratio for this array.

5. Results

A total of 27 MT inversion results were obtained, none of which had been previously investigated. The locations of the analyzed LF seismic events cover the entire area of Mt. Vesuvius, with centroid depths ranging from 4 km to 8 km (see data description in Section 4), and moment magnitudes (M_w) varying from 0.6 to 1.8. The centroid depth is poorly resolved, but in general the depths converge well within the selected depth interval, which was chosen based on previous studies of LP events at Mt. Vesuvius (Galluzzo et al., 2020; Galluzzo et al., 2022). The location of the analyzed events, both in map view and along NS and EW cross sections, and the deviatoric moment tensors estimated in this study are shown in Fig. 4. The hypocenters are mainly distributed in the southern sector of Vesuvius, below the Great Cone. The corresponding hypocentral parameters are given in Table 2, which also shows the number of seismic stations used for the inversion with the best-chosen frequency band and the azimuth gap. Some details of the moment tensor inversion results are shown in Fig. 5 for a selected earthquake (April 3, 2018, M_w 1.1). Fig. 5a shows the moment tensor decomposition for the best and mean MT solution in the frequency band 2–7 Hz (see Table 2). A fuzzy moment tensor representation to highlight the focal mechanism resolution is shown in Fig. 5b, where a small uncertainty is represented by a good separation between black and white quadrants. The red line inside the beachball indicates the solution with the lowest misfit. A comparison of experimental and synthetic data for selected stations and components, both in time (waveforms) and frequency (amplitude spectra) domains, is shown in Fig. 5c. Most of the waveforms and spectra can be well reproduced. The few discrepancies can be attributed to local structural anomalies responsible of site effects not accounted for in our procedure. The focal mechanisms are very heterogeneous. Most of the solutions show normal and strike-slip focal mechanisms, but two thrust mechanisms are also present, such as for the LF event of August 29, 2014, which is characterized by a compressional axis-oriented NW-SE (Fig. 6). The corresponding full moment tensor (FMT) solutions and centroid parameters are provided in Suppl. Material (Fig. S1 and Table S1, respectively). A discussion of the deviatoric moment tensor (DMT) is given in the next section. In general, our analyses show that the source mechanisms are highly heterogeneous with respect to each other, confirming the general results of previous studies

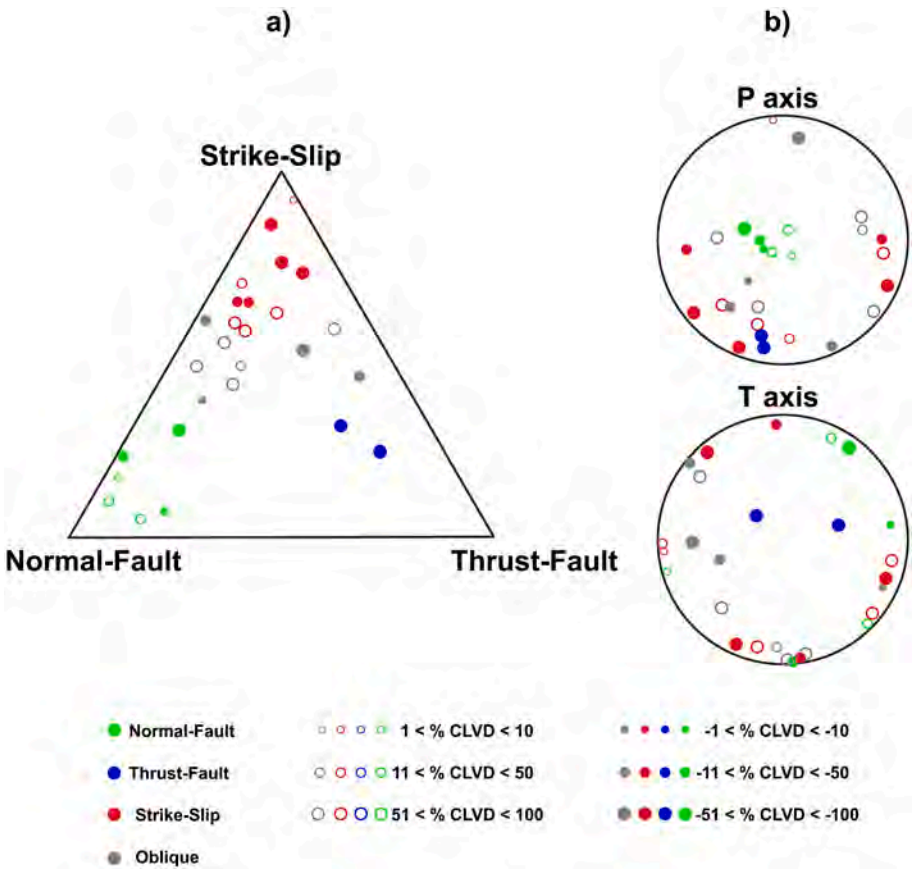

Fig. 7. Overview of the deviatoric moment tensor results. Normal, inverse, strike-slip and oblique focal mechanisms are represented by green, blue, red and grey circles, respectively. The size of the circles is proportional to the percentage of the CLVD component. Positive and negative CLVD percentages are represented by filled and empty circles, respectively. a) Distribution of the focal mechanisms in the Frohlich diagram (Frohlich, 1992). b) Orientation of pressure (P) and tension (T) axes. (For interpretation of the references to colour in this figure legend, the reader is referred to the web version of this article.)

(Bianco et al., 1998; D'Auria et al., 2014; Cusano et al., 2022).

6. Discussion and conclusions

In this section, we only discuss the deviatoric moment tensor (DMT) solutions (Fig. 4 and Table 2) rather than the full moment tensor (FMT) solutions, as they are similar in their deviatoric terms to the DMT solutions, but the isotropic components are poorly resolved (see Table S1 and Fig. S1 in Suppl. Material). Our results indicate a strong heterogeneity of LF seismic sources at Vesuvius for the period 2012–2021. To illustrate the heterogeneity of the moment tensors, we plot them using a Frohlich triangle representation (Frohlich, 1992) (Fig. 7a), and we show the orientation of the pressure (P) and tension (T) axes in separate plots (Fig. 7b). Fig. 7a shows a predominance of normal (green circles) and strike-slip (red circles) mechanisms, whose size is proportional to the percentage of CLVD component. Positive and negative CLVD percentages are represented by filled and empty circles, respectively. In addition, 11 LF events (grey circles) are characterized by oblique focal mechanisms. On the other hand, no preferential direction is observed for either pressure or tension axes (Fig. 7b). The strong heterogeneity of the source mechanisms is also shown by the wide range of the CLVD percentage, which in many cases shows quite high values, both positive and negative. However, it is worth noting that non-double-couple terms are generally poorly resolved (see confidence intervals in Table 2 and Suppl. Table S1), probably due to the low magnitude of the events, the low signal-to-noise ratio of the analyzed signals, the little-known details of the velocity model, the contribution of site effects to the recorded waveforms and the not always available good azimuth coverage (see Table 2.)

The heterogeneity of our MT solutions for LF events is a striking result, especially considering that some of the events with different MTs are separated by a small distance. It is worth noting that the observed differences between the moment tensors are confirmed by the different waveforms for LF events recorded at the same stations. For example, Fig. 8 shows the waveforms of two LF seismic events whose epicenters are ~1 km apart (i.e., the LF seismic events of April 30, 2013, ID 2 in Table 2, and February 28, 2014, ID 9 in Table 2). The former is characterized by a normal focal mechanism, while the latter is described by a strike-slip focal mechanism. Waveforms recorded at 5 seismic stations close to the volcanic cone are shown for both LF seismic events (Fig. 8). The waveforms of the two events are extremely different, consistent with a difference in their focal mechanisms.

To our knowledge, no other seismic source inversions of LF seismic events at Vesuvius are available in the scientific literature, except for a single case by Cusano et al. (2013). Therefore, we attempted to compare our LF focal mechanisms with those of VT events by Bianco et al. (1998), D'Auria et al. (2014) and Cusano et al. (2022). First, some differences between the above studies should be highlighted. Bianco et al. (1998) discuss focal mechanisms for VT events at Vesuvius from 1992 to 1999, D'Auria et al. (2014) refer to VT events from 1999 to 2014, and Cusano et al. (2022) report VT focal mechanisms from 2018 to 2020. In addition, it should be noted that in the three mentioned studies, the focal mechanisms were calculated using both different methods and velocity models. Fig. 9 shows the comparison between the focal mechanisms obtained in this study for LF seismic events and those of VT earthquakes from previous studies, with the aim of providing a more comprehensive overview of the source of Vesuvius seismicity over the last 30 years. For a better visualization, red, orange and purple colours are assigned to the

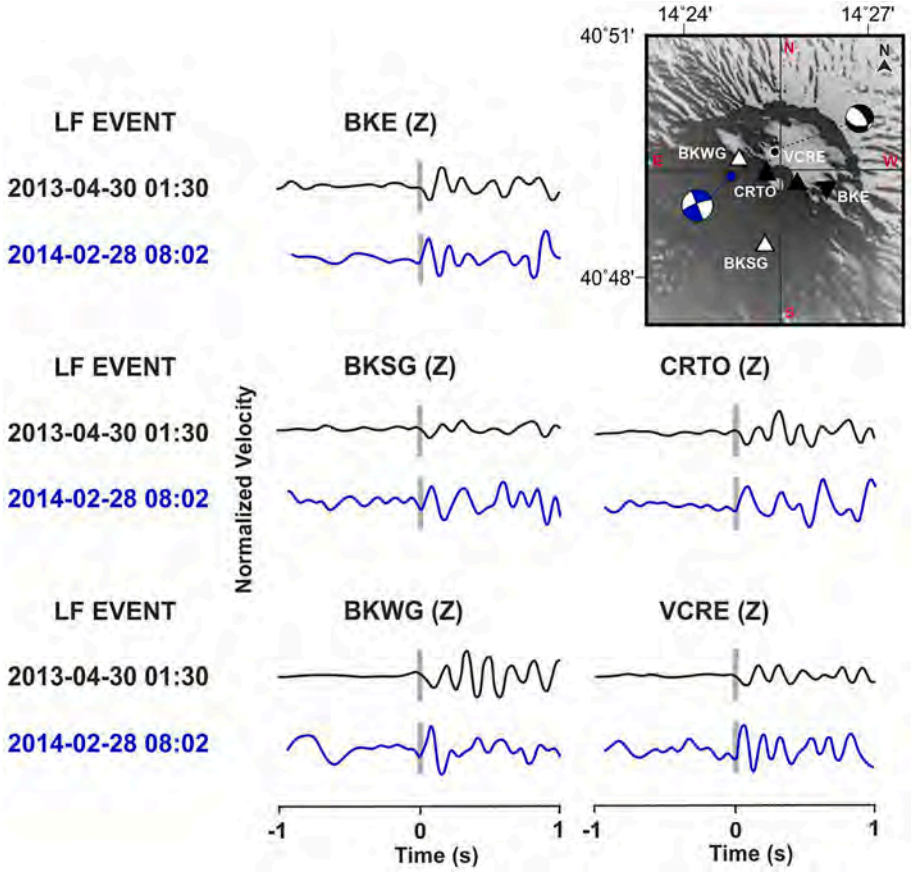

Fig. 8. The hypocenters of the LF seismic events that occurred on April 30, 2013 (ID 2 in Table 2) and February 28, 2014 (ID 9 in Table 2), are represented by black and blue circles, respectively. The focal mechanisms are represented by black and blue beachballs, respectively. The waveforms of the two selected events are shown in black and blue, respectively. The manual picking of the presumed P-phase arrival is represented by a thin grey band. (For interpretation of the references to colour in this figure legend, the reader is referred to the web version of this article.)

results by Bianco et al. (1998), D'Auria et al. (2014) and Cusano et al. (2022), respectively. The VT focal mechanisms in the Frohlich triangle (Frohlich, 1992) from the three mentioned papers are shown in Figs. 8a, d and g, respectively. The results of Bianco et al. (1998) show a prevalence of strike-slip mechanisms, with lower percentages of normal- and inverse-type mechanisms. D'Auria et al. (2014) analyzed about 200 VT events with focal mechanisms distributed across all three competence areas of the triangle diagram. Similarly, the VTs analyzed by Cusano et al. (2022) show all types of mechanisms. Therefore, the volcano-tectonic seismicity from 1992 to approximately the present is characterized by a strong heterogeneity in terms of focal mechanisms in all the works of the cited authors. Figs. 8b, e and h show the pressure (P) and tension (T) axes for the solutions of the three references. Even the latter results do not indicate any preferential direction. Finally, Figs. 8c, f and i show the depths of the hypocenters associated with the three papers under consideration. Bianco et al. (1998) analyse VT seismic events located at depths between 0 and 5 km b.s.l. Conversely, D'Auria et al. (2014) focus on 200 seismic events located at depths ranging from 1 km a.s.l (above sea level) to 7 km b.s.l. Lastly, the hypocenters of the VT events analyzed by Cusano et al. (2022) are located at depths up to 4 km b.s.l.

None of the cited authors identify LF seismic events. However, D'Auria et al. (2014) recognized a bimodal hypocentral distribution with a second family of deeper events that could correspond to our LF events. On the other hand, studies of LF at Mt. Vesuvius had not been identified as such until then. To demonstrate the reliability of the inversion results of LF events, we applied our inversion approach to the focal mechanisms of VT events estimated by the above-mentioned authors (Fig. S2 in the Suppl. Material). Specifically, were considered the most energetic VT seismic events ($M_D > 2.0$) by D'Auria et al. (2014) and Cusano et al. (2022). Again, for better visualization, orange, purple and black colours are assigned to the results by D'Auria et al. (2014), Cusano et al. (2022) and the current study, respectively. For all case studies, our approach shows VT focal mechanisms in agreement with those of the previous authors (see Fig. S2 in the Suppl. Material). In summary, shallow seismicity (up to ~4 km b.s.l.) can be attributed to the downward lithostatic pressure exerted by the volcano itself (Bianco et al., 1998). Deep seismicity caused by combinations of VT and LF seismic sources can be attributed to the superposition of a lower velocity fluid layer. The latter hypothesis is supported by other geophysical studies, such as active seismic tomography (Auger et al., 2001 and references therein) and magnetotelluric surveys (Di Maio et al., 1998), which have identified a low–seismic velocity and high–electrical conductivity layer approximately beneath the central Vesuvian apparatus at a depth of about 8 km, extending in an *E*-W direction, which both authors attribute to a melting zone.

Our study highlights the dormant status of Mt. Vesuvius, a volcano characterized by very few LF-type events in the last 30 years. The low number of LF events compared to the shallow VT-type events does not allow us to establish a proper relationship between the two seismic families. In addition, we note that Mt. Vesuvius is characterized by LF-type events with special features, and thus behaves in a different way from many other volcanoes in the world that erupted during the instrumental epoch. This is the case of Mt. Etna in southern Italy, where LF events have been analyzed using a full waveform inversion between 0.2 Hz and 1.3 Hz (Lokmer et al., 2007; De Barros et al., 2011). These

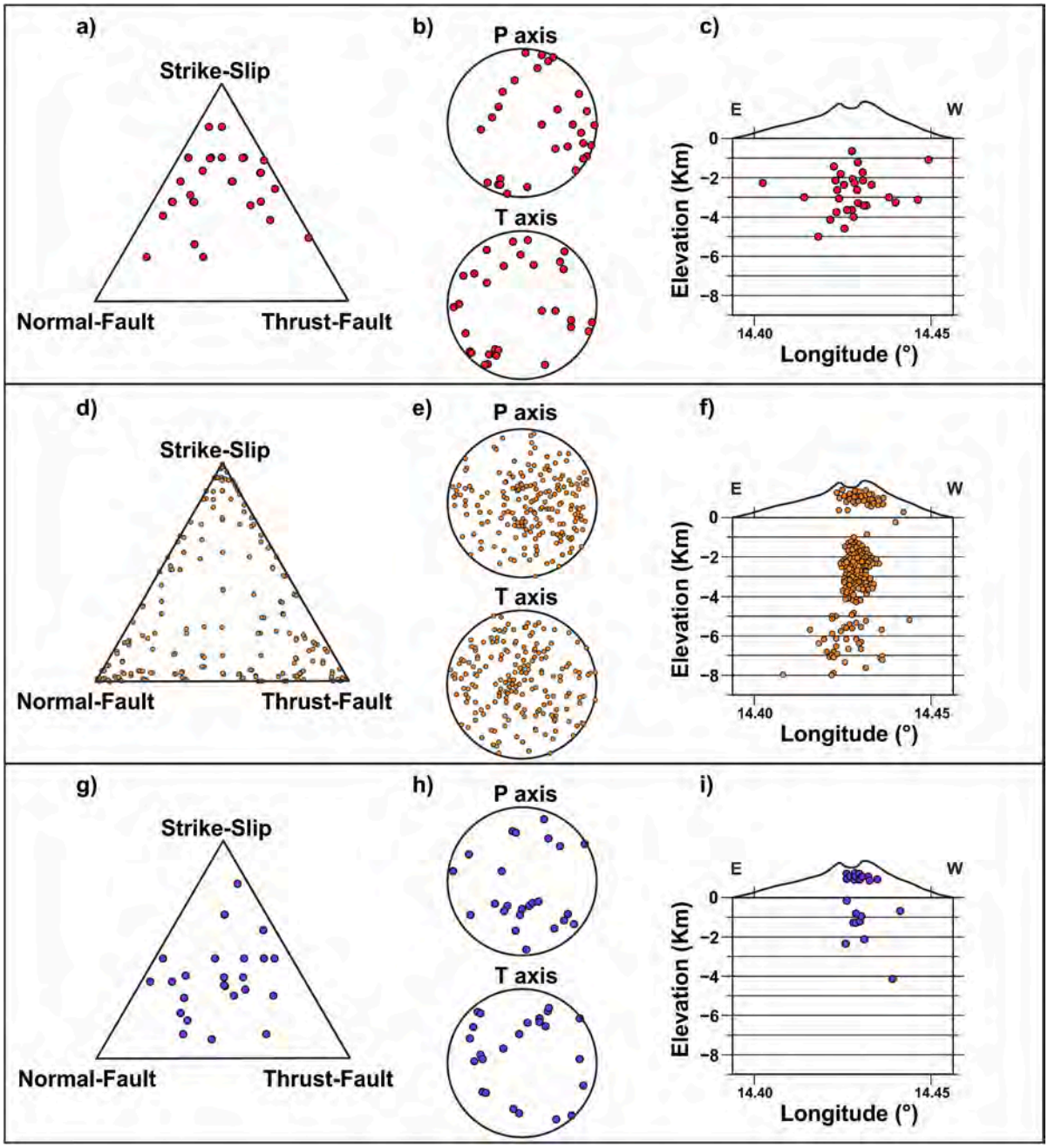

Fig. 9. Summary of VT event solutions retrieved from Bianco et al. (1998), D'Auria et al. (2014) and Cusano et al. (2022), represented by red, orange and purple colours, respectively. a), d) and g) Distribution of the focal mechanisms in the Frohlich diagram (Frohlich, 1992). b), e) and h) Orientation of pressure (P) and tension (T) axes of the corresponding focal mechanisms. c), f) and i) Centroid distribution of VT events of the reference authors in the EW section. (For interpretation of the references to colour in this figure legend, the reader is referred to the web version of this article.)

signals are characterized by a seismic moment of the order of 5×10^{11} Nm recorded by seismic stations in a distance range < 2 km. The same is true for Mount St. Helens (Waite et al., 2008), where the LFs ($M_L < 2.0$) analyzed by a full waveform inversion are recorded by seismic stations at distance <5 km. Different frequency ranges (0.8–5 Hz) have been used for Kusatsu-Shirane volcano in Japan (Nakano and Kumagai, 2005), where LFs are recorded by seismic stations at very short distance <1 km. The seismicity framework we provide for Mt. Vesuvius is very different from that of the volcanoes mentioned above. A volcano characterized by a completely opposite dynamics is the Lascar in Chile (Gaete et al., 2019). In fact, in this case, deep seismicity is characterized by VT events due to fracturing of the rock at depth and magma rises along preferential routes and fractures. The oscillation of fluids in the surrounding fractured rocks causes LF-type seismic events in the shallow part of the volcano, characterized by highly homogeneous focal mechanisms.

Beyond a comparison of LF and VT kinematics, our review of previous works on Mt. Vesuvius provides, for the first time, an overview of the seismicity features over the entire depth range. Away from any differences between VT and LP rupture processes and the depth extent of the seismogenic region, this comparison confirms a strong heterogeneity in the fault geometry and the driving stress field of seismicity at Mt. Vesuvius over the last 30 years.

The results obtained in this work, using a probabilistic methodology based on signal similarity in the time and frequency domain, have proved fundamental to the analysis of the source mechanism of the deep,

low-amplitude earthquakes that have occurred at Mt. Vesuvius, and suggest the application of the proposed procedure to similar volcanic areas characterized by low-energy seismicity.

CRediT authorship contribution statement

R. Manzo: Writing – review & editing, Writing – original draft, Visualization, Validation, Methodology, Investigation, Formal analysis, Data curation, Conceptualization. **S. Cesca:** Writing – review & editing, Writing – original draft, Visualization, Validation, Supervision, Software, Methodology, Formal analysis, Data curation, Conceptualization. **D. Galluzzo:** Writing – review & editing, Writing – original draft, Visualization, Validation, Supervision, Project administration, Conceptualization. **M. La Rocca:** Writing – review & editing, Writing – original draft, Visualization, Validation. **M. Picozzi:** Writing – review & editing, Writing – original draft, Visualization, Validation. **R. Di Maio:** Writing – review & editing, Writing – original draft, Visualization, Validation, Supervision, Project administration, Conceptualization.

Declaration of competing interest

The authors declare that they have no known competing financial interests or personal relationships that could have appeared to influence the work reported in this paper.

Data availability

Data will be made available on request.

Appendix A. Supplementary data

Supplementary data to this article can be found online at https://doi.org/10.1016/j.jvolgeores.2024.108173.

References

Andronico, D., Calderoni, G., Cioni, R., Sbrana, A., Suplizio, R., Santacroce, R., 1995. Geological map of Somma–Vesuvius Volcano. Period. Mineral. 64, 77–78.

Auger, E., Gasparini, P., Virieux, J., Zollo, A., 2001. Seismic evidence of an extended magmatic sill under Mt. Vesuvius. Science 294, 1510–1512.

Bernasconi, A., Bruni, P., Gorla, L., Principe, C., Sbrana, A., 1981. Risultati preliminari dell'esplorazione geotermica profonda nell'area vulcanica del Somma-Vesuvio. Rend. Soc. Geol. Ital. 4, 237–240.

Bianco, F., Castellano, M., Milano, G., Ventura, G., 1998. The Somma-Vesuvius stress field induced by regional tectonics: evidences from seismological and mesostructural data. J. Volcanol. Geotherm. Res. 82, 199–218.

Brancaccio, L., Cinque, A., Romano, P., Rosskopf, C., Russo, F., Santangelo, N., Santo, A., 1991. Geomorphology and neotectonic evolution of a sector of the Tyrrhenian flank of the Southern Apennines (region of Naples, Italy). Zeitsch. Geomorphol. Suppl. Issues 82, 47–58.

Brocchini, D., Principe, D., Castradori, M., Laurenzi, A., Gorla, L., 2001. Quaternary evolution of the southern sector of the Campania Plain and early Somma-Vesuvius activity: insights from the Trecase 1 well. Mineral. Petrol. 73, 67–91.

Büyükakpinar, P., Cesca, S., Heimann, S., Kühn, D., López-Comino, J.Á., Dahm, T., 2023. Source mechanisms of the 2020 volcano-tectonic swarm on the Reykjanes Peninsula (Iceland) by probabilistic moment tensor inversion. In: XXVIII General Assembly of the International Union of Geodesy and Geophysics (IUGG). GFZ German Research Centre for Geosciences.

Chouet, B.A., 1996. Long-period volcano seismicity: its source and use in eruption forecasting. Nature 280, 309–316.

Chouet, B.A., 2003. Volcano seismology. Pure Appl. Geophys. 160, 739–788.

Chouet, B.A., Page, R., Stephens, C., Lahr, J., Power, J., 1994. Precursory swarms of long-period events at Redoubt Volcano (1989-1990), Alaska: their origin and use as a forecasting tool. J. Volcanol. Geotherm. Res. 62, 95–135.

Cusano, P., Petrosino, S., Bianco, F., Del Pezzo, E., 2013. The first long period earthquake detected in the background seismicity at Mt. Vesuvius. Ann. Geophys. 56, S0440.

Cusano, P., Ricco, C., Aquino, I., Petrosino, S., 2022. A first step towards the definition of a link between ground tilt and earthquakes at Mt. Vesuvius (Italy). Appl. Sci. 12, 12261.

D'Auria, L., Esposito, A.M., Lo Bascio, D., Ricciolino, P., Giudicepietro, F., Martini, M., Caputo, T., De Cesare, W., Orazi, M., Peluso, R., 2013. The recent seismicity of Mt. Vesuvius: inference on seismogenic processes. Ann. Geophys. 56, S0442.

D'Auria, L., Massa, B., Matteo, A., 2014. The stress field beneath a quiescent stratovolcano: the case of Mount Vesuvius. J. Geophys. Res. 119, 1181–1199.

De Barros, L., Lokmer, I., Bean, C.J., O'Brien, G.S., Saccorotti, G.S., Métaxian, J.-P., Zuccarello, L., Patanè, D., 2011. Source mechanism of long-period events recorded by a high-density seismic network during the 2008 eruption on Mount Etna. J. Geophys. Res. 116, B01304 https://doi.org/10.1029/2010JB007629.

Del Fresno, C., Cesca, S., Klügel, A., Cerdeña Domínguez, I., Díaz-Suárez, E.A., Dahm, T., García-Cañada, L., Meletlidis, S., Milkereit, C., Valenzuela-Malebrán, C., López-Díaz, R., López, C., 2023. Magmatic plumbing and dynamic evolution of the 2021 La Palma eruption. Nat. Commun. 14 (1), 358.

Di Maio, R., Mauriello, P., Patella, D., Petrillo, Z., Piscitelli, S., Siniscalchi, A., 1998. Electric and electromagnetic outline of the Mount Soma–Vesuvius structural setting. J. Volcanol. Geotherm. Res. 82, 219–238.

Ferrucci, F., Gaudiosi, G., Pino, N.A., Luongo, G., Hirn, A., Mirabile, L., 1989. Seismic detection of a major Moho up-heaval beneath the Campania volcanic area (Naples, Southern Italy). Geophys. Res. Lett. 6 (11), 1317–1320.

Frohlich, C., 1992. Triangle diagrams: ternary graphs to display similarity and diversity of earthquake focal mechanisms. Phys. Earth Planet. Inter. 75, 193–198.

Gaete, A., Cesca, S., Franco, L., San Martin, J., Cartes, C., Walter, T., 2019. Seismic activity during the 2013–2015 interruptive phase at Lascar volcano, Chile. Geophys. J. Int. 219 (1), 449–463.

Galluzzo, D., Nardone, L., La Rocca, M., Esposito, A.M., Manzo, R., Di Maio, R., 2020. Statistical moments of power spectrum: a fast tool for the classification of seismic events recorded on volcanoes. Adv. Geosci. 52, 67–74.

Galluzzo, D., Manzo, R., La Rocca, M., Nardone, L., Di Maio, R., 2022. Detection of low frequency seismicity at Mt. Vesuvius based on coherence and statistical moments of seismic signals. Appl. Sci. 13 (1), 194.

Giudicepietro, F., Orazi, M., Scarpato, G., Peluso, R., D'Auria, L., Ricciolino, P., Lo Bascio, D., Esposito, A.M., Borriello, G., Capello, M., Caputo, A., Buonocunto, C., De Cesare, W., Vilardo, G., Martini, M., 2010. Seismological monitoring of Mount Vesuvius (Italy): more than a century of observations. Seismol. Res. Lett. 81, 625–634.

Heimann, S., Isken, M., Kühn, D., Sudhaus, H., Steinberg, A., Daout, S., Cesca, S., Vasyura-Bathke, H., Dahm, T., 2018. Grond – A Probabilistic Earthquake Source Inversion Framework V. 1.0, GFZ.

Heimann, S., Vasyura-Bathke, H., Sudhaus, H., Isken, M., Kriegerowski, M., Steinberg, A., Dahm, T., 2019. A Python framework for efficient use of pre-computed Green's functions in seismological and other physical forward and inverse source problems. Solid Earth 10, 1921–1935.

Hyppolite, J., Angelier, J., Roure, F., 1994. A major change revealed by quaternary stress patterns in the Southern Apennines. Tectonophysics 230, 199–210.

Imbò, G., 1952. Annali dell'osservatorio vesuviano. Sesta Ser. 1.

Jost, M.L., Herrmann, R.B., 1989. A student's guide to and review of moment tensors. Seismol. Res. Lett. 60 (2), 37–57.

Julian, B.R., Miller, A.D., Foulger, G.R., 1998. Non-double-couple earthquakes 1 theory. Rev. Geophys. 36 (4), 525–549.

Knopoff, L., Randall, M.J., 1970. The compensated linear-vector dipole: a possible mechanism for deep earthquakes. J. Geophys. Res. 75 (26), 4957–4963.

Kühn, D., Heimann, S., Isken, M., Ruigrok, E., Dost, B., 2020. Probabilistic moment tensor inversion for hydrocarbon- induced seismicity in the groningen gas field, the netherlands, part 1: testing. Bull. Seismol. Soc. Am. 110, 2095–2111.

La Rocca, M., Galluzzo, D., 2014. Seismic monitoring of Mt. Vesuvius by array methods. Seismol. Res. Lett. 85, 809–816.

La Rocca, M., Galluzzo, D., 2015. Seismic monitoring of Campi Flegrei and Vesuvius by stand-alone instruments. Ann. Geophys. 58, 0544.

La Rocca, M., Galluzzo, D., 2016. Volcanic tremor at Mt Vesuvius associated with low frequency shear failures. Earth Planet. Sci. Lett. 442, 32–38.

Lavecchia, G., 1988. The Tyrrhenian–Apennines system: structural setting and seismotectogenesis. Tectonophysics 147, 263–296.

Locardi, E., Nicolich, R., 1988. Geodinamica del tirreno e dell'appennino centromeridionale: la nuova carta della Moho. Soc. Geol. Ital. 41, 121–140.

Lokmer, I., Bean, C.J., Saccorotti, G., Patanè, D., 2007. Moment-tensor inversion of LP events recorded on Etna in 2004 using constraints obtained from wave simulation tests. Geophys. Res. Lett. 34, L22316 https://doi.org/10.1029/2007GL031902.

Lomax, A., Zollo, A., Capuano, P., Virieux, J., 2001. Precise absolute earthquake location under Somma-Vesuvius volcano using a new three-dimensional velocity model. Geophys. J. Int. 146, 313–331.

McNutt, S.R., 2005. Volcanic seismology. Annu. Rev. Earth Planet. Sci. 32, 461–568.

Miller, A.D., Foulger, G.R., Julian, B.R., 1998. Non-double-couple earthquakes 2, Observations. Rev. Geophys. 36 (4), 551–568.

Nakano, M., Kumagai, H., 2005. Waveform inversion of volcano-seismic signals assuming possible source geometries. Geophys. Res. Lett. 32, L12302 https://doi.org/10.1029/2005GL022666.

Neuberg, J., 2000. External modulation of volcanic activity. Geophys. J. Int. 142, 232–240.

Oldow, J.S., D'Argenio, B., Ferranti, L., Pappone, G., Marsella, E., Sacchi, M., 1993. Large-scale longitudinal extension in the southern Apennines contractional belt, Italy. Geology 21, 1123–1126.

Orazi, M., D'Auria, L., Tramelli, A., Buonocunto, C., Capello, M., Caputo, A., De Cesare, W., Giudicepietro, F., Martini, M., Peluso, R., Scarpato, G., 2013. The seismic monitoring network of Mt. Vesuvius. Ann. Geophys. 56, S0450.

Petrosino, S., Cusano, P., 2020. Low frequency seismic source investigation in volcanic environment: the Mt. Vesuvius atypical case. Adv. Geosci. 52, 29–39.

Piochi, M., Bruno, P.P., De Astis, G., 2005. Relative roles of rifting tectonics and magma ascent processes: inferences from geophysical, structural, volcanological, and geochemical data for the Neapolitan volcanic region (southern Italy). Geochem. Geophys. Geosyst. 6, 1–25.

Rosi, M., Principe, C., Vecci, R., 1993. The 1631 Vesuvius eruption. A reconstruction based on historical and stratigraphical data. J. Volcanol. Geotherm. Res. 58, 151–182.
Saccorotti, G., Petrosino, S., Bianco, F., Castellano, M., Galluzzo, D., La Rocca, M., Del Pezzo, E., Zaccarelli, L., Cusano, P., 2007. Seismicity associated with the 2004-2006 renewed ground uplift at Campi Flegrei Caldera, Italy. Phys. Earth Planet. Inter. 165 (1–2), 14.
Santacroce, R., 1987. Somma-Vesuvius, 114. CNR, Rome, Italy, p. 249.
Saraò, A., Panza, G.F., Privitera, E., Cocina, O., 2001. Non-double-cpuple mechanisms in the seismicity preceding the 1991-1993 volcano eruption. Geophys. J. Int. 145, 319–335.
Saraò, A., Cocina, O., Privitera, E., Panza, G.F., 2010. The dynamics of the 2001 Etna eruption as seen by full moment tensor analysis. Geophys. J. Int. 181 (2), 951–965.
Spadini, G., Wezel, F.C., 1995. Structural evolution of the '41st parallel zone': Tyrrhenian Sea. Terra Nova 6, 552–562.
Stein, S., Wysession, M., 2003. Introduction to Seismology, Earthquakes and Earth Structure. Blackwell Publishing, Oxford, p. 498.
Templeton, D.C., Dreger, D.S., 2006. Non-double-couple earthquakes in the Long Valley volcanic region. Bull. Seismol. Soc. Am. 96 (1), 69–79.
Ventura, G., Vilardo, G., 1999. Slip tendency analysis of the Vesuvius faults: implication for the seismotectonic and volcanic hazard assessment. Geophys. Res. Lett. 26 (21), 3229–3232.
Waite, G.P., Chouet, B.A., Dawson, P.B., 2008. Eruption dynamics at Mount St. Helens imaged from broadband seismic waveforms: interaction of the shallow magmatic and hydrothermal systems. J. Geophys. Res. 113, B02305 https://doi.org/10.1029/2007JB005259.
Wang, R., 1999. A simple orthonormalization method for stable and efficient computation of Green's functions. Bull. Seismol. Soc. Am. 89, 733–741.
Wassermann, J., 2009. Volcano Seismology. New Manual of Seismological Observatory (Practice-NMSOP).
Zobin, V.M., 2012. Introduction to Volcanic Seismology. Elsevier.
Zollo, A., Marzocchi, W., Capuano, P., Lomax, A., Iannaccone, G., 2002. Space and time behaviour of seismic activity and Mt. Vesuvius volcano, Southern Italy. Bull. Seismol. Soc. Am. 92 (2), 625–640.